Journal of Marine Research, 77, 353–374, 2020

Deep circulation in the Lau Basin and Havre Trough of the western South Pacific Ocean from floats and hydrography

by Elizabeth Simons[1], Kevin Speer[1,2,3], and Andreas M. Thurnherr[4]

ABSTRACT

A system of meridional ridges in the western South Pacific Ocean frame the Lau Basin and Havre Trough, and form a barrier to direct communication between the far western South Pacific basins and the interior South Pacific Ocean. The eastern side of this system comprises the Tonga and Kermadec Ridges, the location of the main deep western boundary current entering the Pacific Ocean. Observations from floats released in the Lau Basin as part of the RIDGE2000 program suggested the presence of a western boundary current along the Lau Ridge exiting into the North Fiji Basin. Those observations, together with Argo sub-surface float data and repeat hydrographic sections, confirm and expand the boundary current observations along the Lau Ridge throughout the Lau Basin and into the Havre Trough, along the Colville Ridge. The observations also reveal two previously unrecognized westward flowing jets bisecting the Lau Basin and Havre Trough. Using an extension to the classic Stommel-Arons abyssal circulation model, the predicted strength and location of these boundary currents and their bifurcation is compared with the float observations. The model provides a simplified view of the dynamics controlling the boundary current structure in the deep basins. A comparison of transport within the western boundary current derived from float data, hydrographic sections, and the idealized analytical model indicates that roughly 4 Sv (below 1,000 db) is transported northward through the Lau Basin, exiting into the North Fiji Basin.

Keywords: Deep circulation, Lau Basin, Argo floats, North Fiji Basin, Tonga Ridge, Kermedec Ridge, western boundary currents, South Fiji Basin

1. Introduction

The Kermadec Ridge and Tonga Ridge north of New Zealand form the western boundary of the deep Southwest Pacific Basin north of about 40° S (Fig. 1). Thus, the primary route for the Deep Western Boundary Current (DWBC) system bringing bottom water and Circumpolar Deep Water into the Pacific Ocean is located on the eastern flank of these

1. Geophysical Fluid Dynamics Institute, Florida State University, Tallahassee, FL 32306; orcid: 0000-0002-6260-4833

2. Corresponding author: ***e-mail: kspeer@fsu.edu***

3. Department of Scientific Computing, Florida State University, Tallahassee, FL 32306; orcid: 0000-0001-8294-2832

4. Lamont-Doherty Earth Observatory, Palisades, NY 10964; orcid: 0000-0002-1977-7122

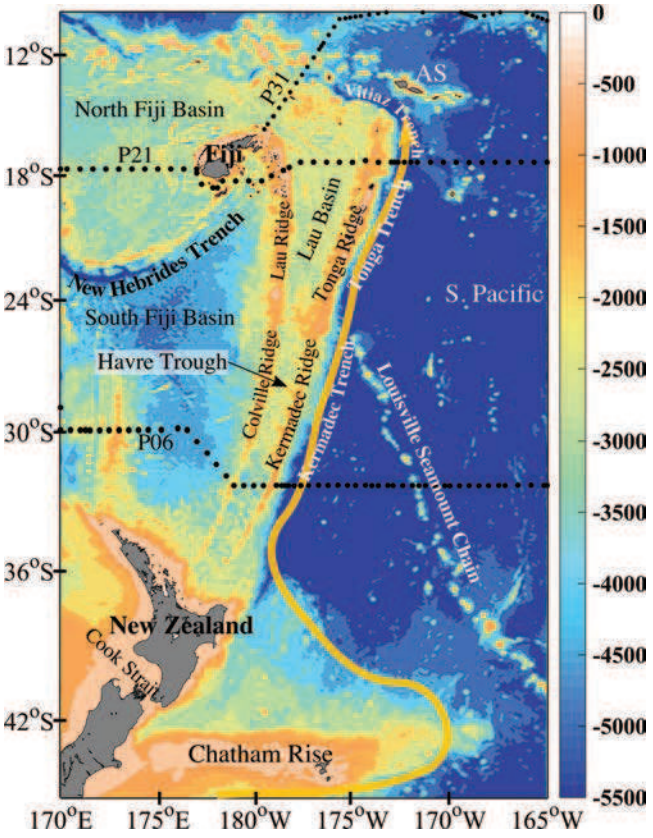

Figure 1. Lau Basin region showing hydrographic stations of the principle World Ocean Experiment and Climate Variability Project sections (P31, P21, P06) and the Deep Western Boundary Current (yellow, adapted from Whitworth et al. [1999]). Bathymetry (m depth) from Smith and Sandwell v19.1.

ridges (Whitworth et al. 1999). They also form a barrier preventing a direct connection from the several basins of the western South Pacific Ocean to the interior South Pacific Ocean, leaving the Tasman Basin, between Australia and New Zealand, as an apparent cul-de-sac for deep South Pacific inflow along the eastern margin of Australia. Small leakages of deep water from the Tasman Basin to basins farther north are thought to occur based on heat budgets (Wyrtki 1961) at levels (0.04 Sv) that are negligible compared with typical circulation transport estimates.

The South Fiji Basin, by contrast, is thought to be supplied with bottom water from the north, with a small, 0.2 Sv, mid-depth source of deep water flowing across sills to the north of New Zealand (Warren et al. 1994). Located between the South Fiji Basin and the interior South Pacific Ocean are the Havre Trough and Lau Basin (Fig. 1). These relatively minor

basins are well known in the geophysical community as active spreading centers hosting numerous hydrothermal vents (Sutton et al. 2012; Tivey et al. 2012). However, they have been largely ignored as components of the regional deep circulation, with emphasis being placed on the nearby western boundary current (WBC) system.

The Lau Basin is bordered on the west by the Lau Ridge and the east by the Tonga Ridge (Fig. 1). The northern boundary of the Lau Basin consists of a series of complicated shoals and small volcanic islands. A southern extension of the basin, called the Havre Trough, is separated from the Lau Basin by a wide sill, about 2,000 m deep near 24° S, and bounded by the Colville Ridge to the west and Kermadec Ridge to the east. The Havre Trough ends where it intersects with New Zealand. Within the Havre Trough, are two small sub-basins, near 28° S and 33° S, respectively, which turn out to play a role in circulation within the trough.

While the routes taken by bottom water are obviously dependent on sills and passages (Warren et al. 1994; Wijffels, Toole, and Davis, 2001), the deep flow (depths greater than 1,000 m) also tends to be guided by the underlying topography constraining potential vorticity (LaCasce 2000). To understand the nature of the exchange between the Lau Basin-Havre Trough system and the surrounding basins and South Pacific Ocean, it is crucial to consider the intricate topographic openings and barriers to flow on the surrounding ridges.

The ridges that form the meridional walls of the Lau Basin and Havre Trough are gap-filled, uneven boundaries (Fig. 2). The Tonga Ridge has multiple ridge breaks, with the deepest ridge breaks at the Tofua Passage (1,900 m) and the Tonga Passage (2,200 m). The Tonga Passage is also the widest passage along the Tonga Ridge, spanning about 200 km. Along the northern portion of the Kermadec Ridge, a set of three shallower openings occur across the Kermadec Passage (1,500 m). Toward the south, sills gradually deepen, with one reaching a depth of about 2,400 m at the base of New Zealand. This sill was noted and exploited by Warren et al. (1994) to infer inflow at 2,000–2,200 m depth to the South Fiji Basin; however, this would require the flow to cross the Colville Ridge, and the deepest sill there is shallower, and lies somewhat farther north, near 32° S (Fig. 2).

At the northern end of the Lau Ridge where it joins the island of Fiji is the North Fiji Passage (depth 2,200 m; Fig. 1), the deepest passage after the analogue junction with the New Zealand plateau at the far southern end of the ridge system. Otherwise, the Lau Ridge remains relatively shallow (above 750 m depth) throughout the Lau Basin. To the south, along the Colville Ridge bordering the Havre Trough, the sill depths increase. The Colville Passage, near 29° S, with depths of 2,000–2,200 m is also relatively wide, about 80 km at 1,500 m depth. It marks the start of a series of deeper passages leading up to an unnamed opening located near 32° S; this latter passage appears to be the deepest passage across the Colville Ridge, at 2,500 m depth. South of this passage, the various sills are shallower right up to the base of the New Zealand continental margin, with maximum depths close to 2,000 m.

The Kermadec Ridge and Tonga Ridge thus form a porous western boundary for the primary deep water inflow to the Pacific Ocean. This inflow, the DWBC, transports about

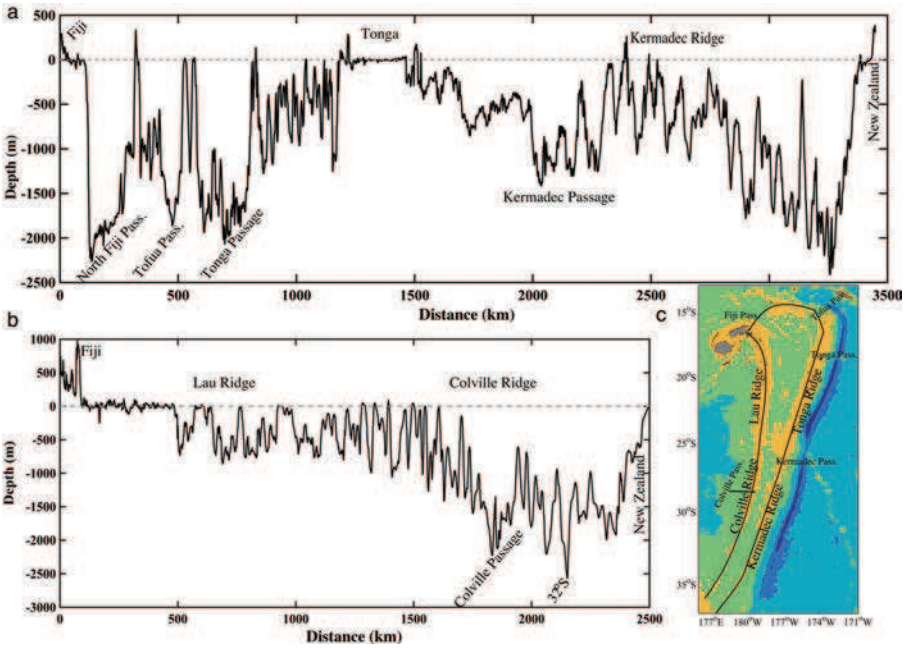

Figure 2. Sill depth along the Tonga and Kermadec Ridges. (a) Sill depth starting at Fiji and ending at the northern island of New Zealand. (b) Sill depth for the Lau and Colville Ridges starting on the southern side of Fiji. (c) Regional map of the area showing the average path where the sill depth was taken.

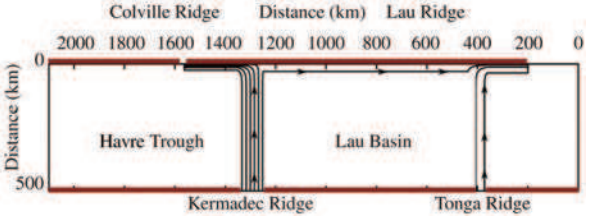

Figure 3. Simple flat-bottom, uniform-layer model of boundary currents and zonal jets. Contours are in units scaled by inflow transport. Arrows indicate direction of the flow. Thick red lines mark the ridge segments.

16 Sverdrups (1 Sv = 10^6m/s) north, of which up to 6 Sv could be carried at depths less than 3,250 m (Whitworth et al. 1999). The upper reaches of the DWBC can potentially supply bottom water to the Havre Trough and South Fiji Basin through the passage at the intersection of the Kermadec Ridge and New Zealand and to the Lau Basin through the Tonga Passage. Warren et al. (1994) noted the possibility of the former but thought that any

flow continued to the South Fiji Basin. The potential supply of deep water from the DWBC through the Tonga Passage has previously remained undocumented.

We derive, for the first time, estimates of deep circulation in the Lau Basin and its southward extension, the Havre Trough. The deep and bottom water circulation is revealed by hydrographic observations from ship-based and Argo float-based data, and from direct velocity estimates based on float trajectories near 1,700 m and 1,000 m depth. A simple model is developed to explain the basic structure of the boundary currents in these basins, and expected and observed transports in the boundary currents are compared. The net result is that deep water enters the Lau Basin across the Tonga Ridge and exits through the North Fiji Passage. However, within the Lau Basin and Havre Trough, observations show an unexpectedly rich deep boundary current network, with a net throughflow of roughly 4 Sv.

Our descriptive study is of intrinsic interest for a region with a poorly known deep circulation. The magnitude of the throughflow makes the Lau Basin a significant contributor to the regional bottom and deep layer transports. The deep circulation is also important in the context of the biogeography of the chemosynthetic organisms associated with the hydrothermal sources in this basin (Van Dover et al. 2002; Desbruyéres, Hashimoto, and Fabri 2006).

2. Methods

a. Data

i. Deep LAUBFLEX floats. As part of the Ridge 2000 Integrated Study Site program in the Lau Basin (Fornari et al. 2012; Tivey et al. 2012), the Lau Basin Float Experiment (LAUBFLEX), 11 APEX (Webb Research, Falmouth MA) and PROVOR (Metocean, Canada) floats were deployed starting in mid-April of 2004, with the last deployment in June of 2005. The deployments were concentrated in the northeastern and central Lau region (Speer and Thurnherr 2012) to study circulation around an active spreading center and hydrothermal vents. Data were reported through March 2011. The floats were equipped to measure temperature and pressure and to maintain a nominal 1,700 db drift depth. The cycle for a LAUBFLEX float consists of a drift period of $\approx$ 21 days at depth, returning to the surface (about 6 hours) to transmit data (about 12 hours) before returning to drift depth. While ascending to the surface, these floats measure only temperature in the water column. On average, during each 21-day cycle, the float spends 36 hours away from the target drift depth.

ii. Argo floats. The majority of Argo floats drift at a nominal depth of 1,000 db and profile the water column vertically from 2,000 db to the surface. The typical float cycle for an Argo float is 10 days with 9 days spent at drift depth before ascending to the surface to transmit data (Ollitrault and Rannou 2013). Floats transmit their data through either Argos systems or Iridium systems. The Argos transmission requires a longer surface stay to transmit all the data (up to 12 hours), whileas Iridium can take as little as 30 minutes of transmission

time. Argo floats measure temperature, salinity, and pressure in the upper 2,000 db. The precision of these measurements and discussion of the evolution of the Argo float can be found in Boyer (2013).

Within the Lau Basin, 152 distinct Argo floats, sourced from the Coriolis global daily assembly center at the French Research Institute for Exploitation of the Sea have passed through the region over 14 years from July 2001 to June 2015. The floats used within this study were primarily APEX floats ($\approx 54\%$) and SOLO floats ($\approx 44\%$) with PROVOR floats making up the difference. See Ollitrault and Rannou (2013) for a full discussion of the float types and differences. The majority of floats used the Argos positioning system through 2005 (Ollitrault and Rannou 2013) and the Iridium positioning system beginning in 2006.

iii. Argo and LAUBFLEX float processing. Following Ollitrault and Rannou (2013), a representative park pressure (RPP) was assigned to each cycle of each Argo float. Assignment of the RPP relies on drift pressure measurements and configuration of park pressure assignments. If several park pressures are measured during a single drift phase, the RPP is the average value of those measurements. If only one number is reported (either as the mean of pressures or a single measurement) that becomes the RPP. If minimum and maximum pressures are given, the RPP is the mean value. When there is no pressure data available, the RPP is assigned from the reported configuration park pressure. This is checked locally, first against the local bathymetry and then against the reasonableness of the induced deep velocity. In the data set used for this study only one float had no measured park pressures and the 1,000 db programmed drift pressure appeared to be compatible with the surrounding bathymetry.

The Argo floats were sorted by drift depth (84% at 1,000 db, 5% below 1,000 db and 11% above), and only floats that had an RPP of between 850–1,250 db were used in the analysis. The Argo floats were a mix of Argos and Iridium based positioning. For further analysis only position data flagged as *3* (position accuracy of < 150 m position uncertainty for Argos), and *gps* (strong connection certainty for Iridium) were used for further velocity calculations and position tracks to limit track position errors once at the surface.

The measurement error encompasses several different points within the Argo cycle. The first point is in the Argos positioning system, with a minimum position uncertainty of $<$ 150 m. Using the mid-range uncertainty of $<$ 1,000 m, Ichikawa et al. (2001) estimates velocity errors of $\mathcal{O}(10^{-3}\frac{m}{s})$ for the 10-day cycle of the float. This error decreases with a decrease in position uncertainty. The second point of error is clock drift, which is considered to be negligible for the majority of floats. Within the data set used for this study, there were no significant clock jumps. The third error arises from the drift associated with ascent and descent. The last error in the velocity estimates is unknown surface drift of the float while waiting for satellite connection and/or descent command. There are upper bound estimates for these errors from several sources (Ichikawa et al. 2001; Lebdev et al. 2007; Katsumata and Yoshinari 2010; Ollitrault and Rannou 2013). Assuming a linear shear profile, Lebdev

(2007) estimates the deep velocity errors at a mean of $5.3 \times 10^{-3} \frac{m}{s}$, with the most probable error around $2.5 \times 10^{-3} \frac{m}{s}$.

The Park et al. (2005) method extrapolates surface and dive positions from the known position-fixes that a float records and the time estimate for an actual surfacing and diving. We use this method for Argo and LAUBFLEX velocity estimates yielding a total velocity uncertainty of $2 \times 10^{-3} \frac{m}{s}$ (Park et al. 2005) independent of the number of floats, requiring three or more surface fixes per surfacing. Velocity fields were estimated from the position tracks and cycle data following the methods outlined in Park et al. (2005), and Gray and Riser (2014). After this processing there were 152 floats with 25,946 velocity estimates used in the study.

All velocities, from Argo floats and LAUBFLEX were mapped onto a $0.25^\circ \times 0.25^\circ$ Eulerian grid, with samples averaged in time bins of three months before fully averaging the area bin. This is to limit the anomalous weighting from multiple observations within a short time frame due to one float occupying a bin for an extended number of continuous samples. The bins were then smoothed using a 2-D convolution filter with a gaussian halfwidth of 75 km (see Float-based circulation). Four or more observations per bin were required for each bin, otherwise the bin velocities were set to an undefined value. It is worth noting that these bin sizes are smaller than have been used in previous studies (Davis 2005; Gray and Riser 2014), which used $1^\circ \times 1^\circ$ bins over larger sections of the Pacific basin. Smaller bin size does increase velocity bias within the bins, but was deemed necessary given initial estimates of the width (25–50 km) of the WBC along the Lau Ridge.

Transports within the Lau Basin were estimated from the float observations. For the float-based estimates, a layer 700 db thick was chosen to match the nominal distance between the Argo floats (1,000 db) and the LAUBFLEX floats (1,700 db). The velocity used for the estimates was the combined mean of the binned data from Argo and LAUBFLEX floats through the Lau Basin. A conservative velocity error of 5mm/s applied to the data set results in a ± 0.35 Sv transport error due to velocity error. Transports within the Havre Trough were estimated from only Argo displacements, since the LAUBFLEX floats did not reach that far south. Net transport for the Havre Trough was estimated using a 700 db thick layer and a reference Argo velocity at 1,000 db with a zero velocity reference at 1,700 db.

b. Hydrographic data

The World Ocean Experiment (WOCE), Climate Variability Project (CLIVAR), and Global Ocean Ship-board Hydrographic Investigations Program (GO-SHIP), produced three hydrographic lines crossing the basin (Fig. 1). At the northern extremity of the Lau Basin, P31 runs from Fiji, northeast, through the Samoan Passage. This hydrographic line has only been occupied once, in 1994, as a component of a mooring array project to study the deep flow through the Samoan Passage (Roemmich, Hautala, and Rudnick 1996). P21 lies nominally along 17.5° S bisecting the Lau Basin, and transects the Pacific Ocean from Australia to the western coast of South America. P21 has been occupied twice, in 1994 and again

in 2009. In the southern limit of the Havre Trough, along 32.5° S, P06 has been repeatedly occupied; this is also the latitude of the PCM9 mooring array, which was deployed to measures the DWBC above the Kermadec Trench (Whitworth et al. 1999). P06 has been occupied four times, in 1992, 2003, 2009, and 2017.

Conductivity, temperature, and depth (CTD) data were used for geostrophic velocity estimates relative to the 1,000 db data set from Argo. The CTD data were processed using only data flagged as the most confident; all other values were deleted and filled by interpolation using a Laplacian filter. The data were then re-interpolated (in the lateral direction) linearly onto a uniform grid, slightly finer than the original horizontal spacing. A dynamic-height based streamfunction was calculated using absolute salinity and conservative temperature, following the Thermodynamic Equation of Seawater-10 (TEOS-10) standard, referenced to 1,000 db. The geostrophic velocity was then estimated, referenced to the 1,000 db velocity field from the processed Argo floats that were within one bin (.25°) of the hydrographic line. The P06 geostrophic velocity was based on a 2,000 db reference level due to the lack of floats, Argo or LAUBFLEX, in that region. Property distributions were used to support the choice of 2,000 db. (See Geostrophic velocity and transport estimates.)

The geostrophic velocity is found using

$$\mathbf{k} \times \nabla_{surf} \Psi = f(\mathbf{v}_{geo} - \mathbf{v}_{ref}). \tag{1}$$

The geostrophic velocity is

$$\mathbf{v}_{geo} = \frac{1}{f}(\mathbf{k} \times \nabla_{surf} \Psi + f\mathbf{v}_{ref}), \tag{2}$$

where $\mathbf{v}_{geo}$ is the geostrophic velocity vector, Ψ is the dynamic height streamfunction, f is the Coriolis parameter and $\mathbf{v}_{ref}$ is the reference velocity, in this case referenced to the 1,000 db Argo velocity data, or a 2,000 db level of no motion. ∇_{surf} becomes ∇_p, since the dynamic height is referenced to a pressure surface.

Net transport estimates below 1,000 db were made from the $\mathbf{v}_{geo}$ estimates on P31 and P21, and below 2,000 db on P06. The flow field was integrated laterally from the western ridge to the eastern ridge and vertically every 2 db. For hydrographic section P31, the flow field was integrated from Fiji northeast for 210 km to a shallow shoal, and vertically every 2 db. Error associated with the geostrophic velocity estimate comes from the reference velocity error (.35 Sv); instrument error is negligible.

3. Results

a. Circulation

i. Float-based circulation. The LAUBFLEX floats were the first observations to indicate a possible narrow (25–50 km wide) WBC along the Lau Ridge (Fig. 4a), with northward velocities of 6–7 cm/s and interior flows as strong as 3 cm/s but typically much weaker (Speer and Thurnherr 2012). This current is evident from 21° S to 18° S, apparently disappears,

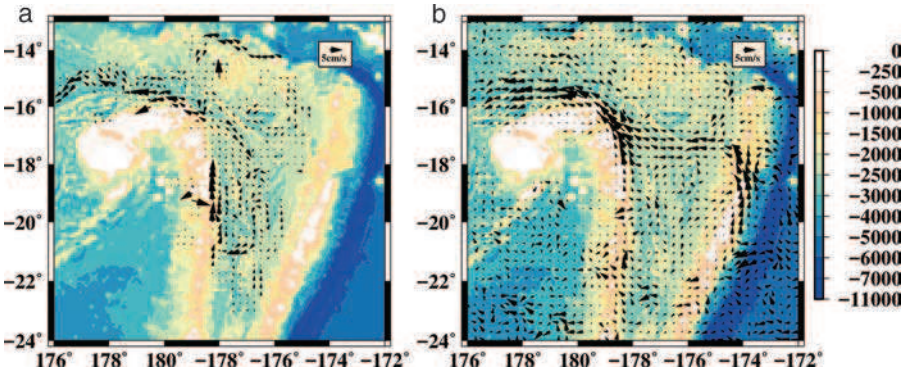

Figure 4. Binned velocities from Lau Basin Float Experiment (LAUBFLEX) and Argo floats (color represents depth in m). (a) LAUBFLEX velocity at 1,700 db. (b) Argo velocity at 1,000 db. A westward jet is evident crossing the Lau Basin at 17° S.

and then re-appears from about 16° S until it exits into the North Fiji Basin through the North Fiji Passage. The gap is likely due to the sampling criteria of this analysis requiring at least four observations per bin. With relatively large velocities, the long float cycle of the LAUBFLEX floats, and fewer floats, bins are undersampled. Inflow north of the North Fiji Passage is associated with a recirculation in the northern Lau Basin, flowing along a deep subsidiary ridge.

Argo displacement data (Fig. 4b) in the area corroborate the DWBC along the Lau Ridge and indicate that the current extends vertically, from 1,700 db to 1,000 db. The Argo data also yield a larger area coverage and indicate several other elements of the circulation in the Lau Basin (Fig. 5). The latitudinal extent of the boundary current in the Lau Basin is indicated by the fairly consistent northward flow from around 26° S through to the North Fiji Passage with velocities of 4–7 cm/s. At 26° S, a bifurcation in the flow leads to a southward flowing boundary current spur from about 26° S to about 30° S. Second, two westward jets are evident, one in the northern portion of the Havre Trough at 26° S and one in the northern portion of the Lau Basin at about 17° S. These two jets align with breaks in the ridge systems: the Tonga Passage (north) and the Kermadec Passage (south). Due to the bifurcation in the boundary current, there are also at least two outflow passages, the Colville Passage in the south, and the North Fiji Passage in the north. Another relatively strong current flows along the Tonga Ridge, feeding the Tonga Passage source into the Lau Basin.

We find two relatively strong areas of recirculation, one in the central Lau Basin centered near 19° S, more evident in the LAUBFLEX data (Fig. 4a), and another in the northern portion of the Havre Trough, centered near 30° S, more evident in the Argo data (Fig. 5). Both of these recirculation systems roughly follow constant geostrophic contours of large scale potential vorticity contours ($\frac{f}{h}$, where f is the Coriolis parameter and h is the thickness of the water column below 1,000 m depth). Within the Havre Trough the sense of the

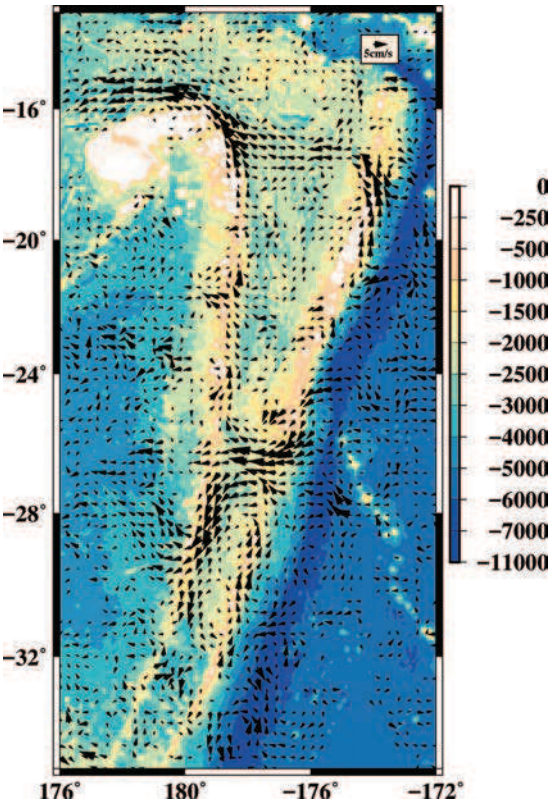

Figure 5. Argo velocity. Two westward jets are located at 17° S and 26° S. The bifurcation along the Colville Ridge, in which part of southern jet turns northward while the majority flows south, is located near 26° S. The northward flowing boundary current exits the Lau Basin through the North Fiji Passage near 16° S.

circulation is anticyclonic, consistent with the embracing boundary current flow, with a northward return arm along the Kermadec Ridge. In the central Lau Basin the recirculation is cyclonic, with some of the WBC water returning southward within the central Lau Basin. A weaker anticyclonic recirculation is evident in the northern Lau Basin.

ii. Circulation based on hydrographic properties. Potential temperature is lowest on station 84 from P06 (2017), in the Havre Trough, at 1.853°C, with the minimum potential temperature increasing to 1.947°C on P21 (2009); temperature is lower again on P31 at 1.885°C (Fig. 6). The Havre Trough P06 potential temperature-salinity relation converges to the South Fiji Basin relation, within error, below about 2°C (Fig. 7), showing that the source of bottom water is the South Fiji Basin. This confirms the supposition of Wyrtki

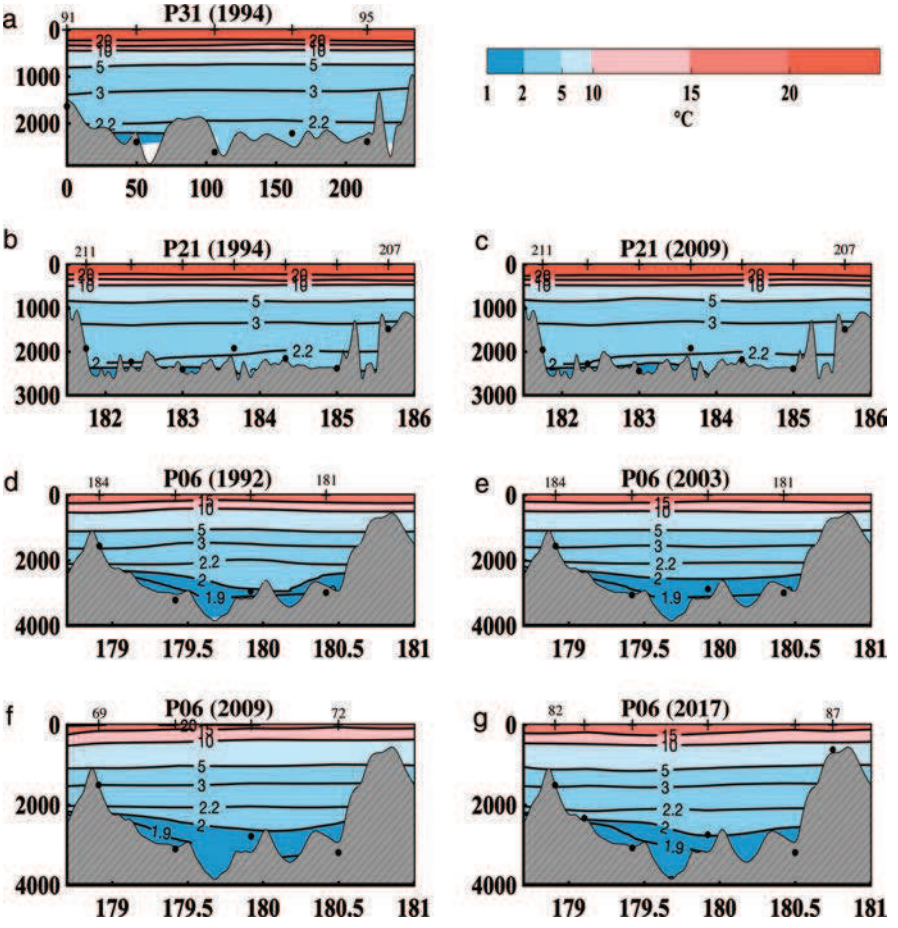

Figure 6. Potential temperature for each hydrographic section and occupation (year) in the Lau Basin and Havre Trough. Black dots mark the maximum pressure during a conductivity, temperature, and depth cast at each station. P31 x-axis is distance in km, depth in m.

(1961), who had no data within the Havre Trough, that the Havre Trough is a minor dependent basin of the South Fiji Basin. On the other side of the Colville Ridge in the South Fiji Basin, bottom potential temperature is 1.545°C. These results suggest that the sill near 32° S (Fig. 2) supplies the Havre Trough, at least as far as the rise separating the Havre Trough from the Lau Basin. This 32° S sill is slightly deeper than the saddle between New Zealand and the Kermadec Ridge. Warren et al. (1994) observed the Havre Trough near this latter sill and found the coldest bottom water there to be 2.0°C.

The temperature of the eastern side of the Havre Trough on P06 at 1.925°C (Fig. 6d-g) is slightly warmer than the western side. The more recent occupations show somewhat higher temperatures. Silica concentration (Fig. 8d-g) is slightly lower in the east, and higher on the

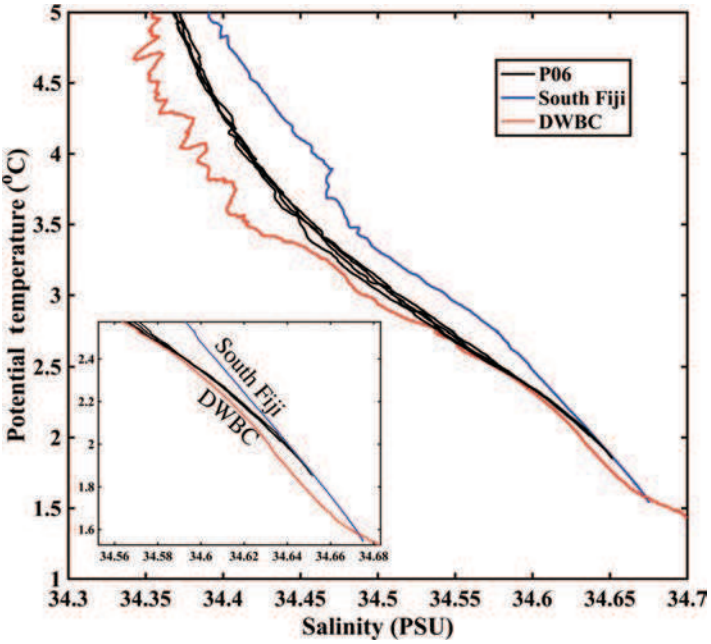

Figure 7. T-S plot of hydrographic stations from P06 (2017) in the southern Havre Trough. A representative Deep Western Boundary Current (DWBC) station and South Fiji Basin station are also shown.

western side of the trough, but only by about 2 μmol/kg; oxygen concentrations (not shown) are indistinguishable across the bottom, with a value near 154 μmol/kg. These properties are similar to those outside the trough at 2,400–2,500 m, and consistent with both a South Fiji Basin source and some mixture of water from the DWBC entering at the saddle on the Kermadec Ridge, whose flow is blocked by the shallower sill on the Colville Ridge, thus turning that inflow north toward the P06 line.

The minimum observed temperature on P21, 1.947°C, occuring on the western side of the basin, corresponds to higher silica (Fig. 8b,c). The coldest bottom water on P31, at the northern limit of the basin, also occurs on the western side of the section. The water in northern Lau Basin evidently comes from the north and first enters an area of anticyclonic recirculation. This recirculation branches at 17° S, such that one branch carries similar properties to the western side of P21. Bottom water properties in the northern Lau Basin thus arrive from the north, through the northeastern side of the North Fiji Passage, and participate in the recirculation in this area. The role of the Tonga Passage as a source of bottom water is unclear, as properties at the closest stations (on P21) do not suggest a nearby source.

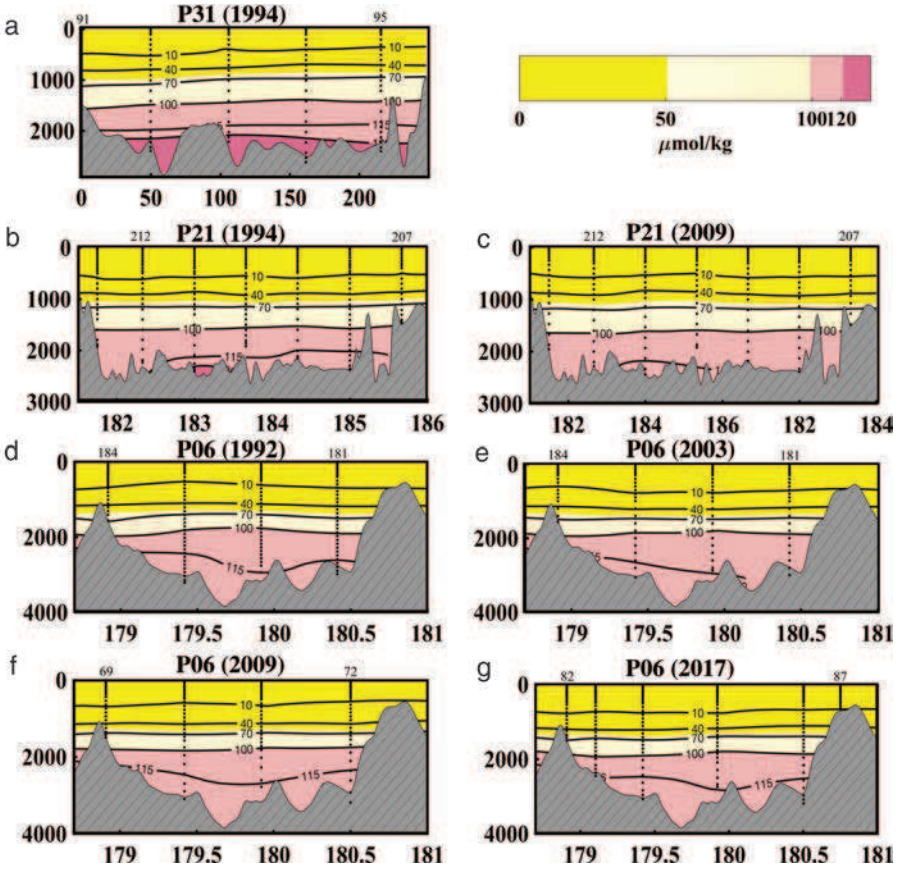

Figure 8. Silica observations for each hydrographic section and occupation (year) in the Lau Basin and Havre Trough. Black dots mark every bottle stop during a conductivity, temperature, and depth cast at each station.

b. Geostrophic velocity and transport estimates

i. North Lau Basin. Along hydrographic line P31, a strong (8 cm/s) north-northwestward flow is evident below 1,000 db hugging a portion of the Fiji Island bathymetry and extending close to 100 km northeast (Fig. 9a). There is a slower (1 cm/s) southeastward flow outside the boundary flow, to just past 200 km. A small opposing flow is observed beyond that, near a complicated bathymetric area just west of the Vitiaz Trench. Circulation in the upper 1,000 db is roughly consistent with Reid's (1997) steric height maps above 1,000 db. Closer to the Fiji plateau, though, the flow is directed south-southwest, perhaps in relation to local effects of the plateau.

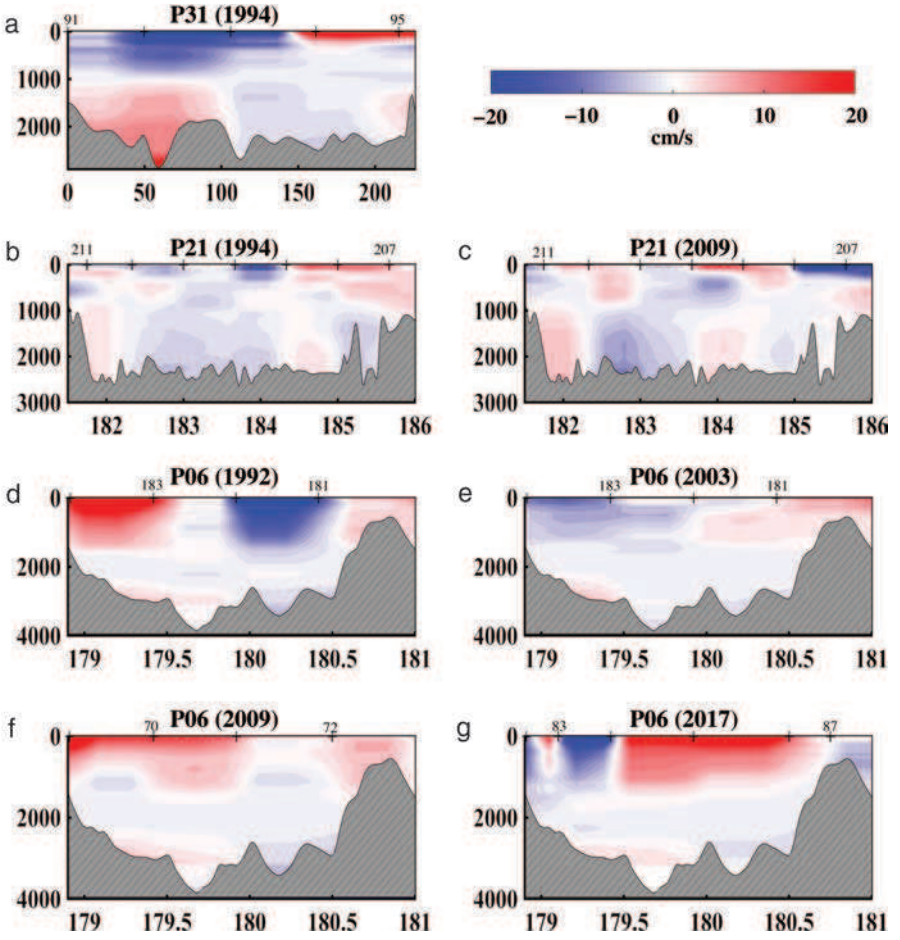

Figure 9. Geostrophic velocity for each hydrographic section and occupation in the Lau Basin and Havre Trough. P31 x-axis distance in km.

Comparing the calculations based on hydrography with the LAUBFLEX deep float velocities, the maximum geostrophic velocities are larger by about a factor of two than the (averaged) float velocities; averaging the geostrophic velocity vertically brings them into closer agreement. Velocity comparisons are more subject to error from synoptic hydrographic sections, however. The hydrography also suggests a wider DWBC (100 km) than do the floats (50 km). The wider DWBC and larger velocities in the hydrographic data are balanced out by more internal structure, and thus produce a net transport similar to that of the floats. A net transport estimate below 1,000 db from the geostrophic flow (see Hydrographic data) results in 5.9 Sv $\pm$ 1 Sv exiting the Lau Basin region. Comparison with transport estimates

from the floats (Argo and LAUBFLEX), 5.6 Sv ± 1 Sv, indicates that the transport estimates agree on a relatively large transport out of the Lau Basin.

ii. Lau Basin. Along P21, there is a strong (8–9 cm/s) and narrow (about 70 km) northward flow along the Lau Ridge from 750 db to below 2,000 db (Fig. 9b, c). This northward flow is trapped to the Lau Ridge with its strongest flow centered between 1,500 and 2,000 db. The southward flow that occurs east of the boundary current has speeds of 4–6 cm/s, is relatively wide (≈ 160 km)for the Lau Basin, and is mostly seen below 1,000 db depth.

From about 183.5° E and eastward to the Tonga Ridge along P21 are two alternating flows, one weak (< 1 cm/s) and one narrow (50–75 km). Near the Tonga Ridge is a deep southward inflow. Both occupations of P21 show similar patterns, though the first occupation in 1994 indicates a narrower (≈ 50 km), and slower (5–6 cm/s) northward flow next to the Lau Ridge.

Comparison with the LAUBFLEX results along the P21 17.5° S line shows that the WBC is weaker in the float observations, ≈ 1 cm/s, versus 5 cm/s or so in the geostrophic fields. Outside (east) of the boundary the LAUBFLEX float trajectories do, however, indicate an inflow region consistent with the geostrophic calculations, but with smaller associated velocities. The net transport estimates yield relationships similar to those for P31. The net transport of P21 in the 1994 occupation is 3.7 Sv ± 1 Sv northward and in the P21 2009 occupation is 4.1 Sv ± 1 Sv northward, in acceptable agreement with the float-based net transport of 4.9 Sv ± 1 Sv northward. Again, just as noted for the North Lau Basin, the hydrographic data show more complicated interior circulation patterns not illustrated in the available float data.

iii. Southern Havre Trough. P06 hydrography indicates, consistently, a deep northward flow along the Colville Ridge within the Havre Trough (Fig. 9d-g). Initially, this was somewhat surprising, given the source passage to the north of the P06 section. At this location the flow shows smaller scale vertical structure; the apparent minimum in vertical shear near 2,000 db depth led us to choose that depth as a zero velocity reference level. With this choice the core of the flow appears to be aligned with the observed weak property variations. The bottom properties are consistent with inflow from the South Fiji Basin, with shallower levels receiving some component of water from the southern end of the Kermadec Ridge, though we are unable to make much of a distinction between the western and eastern sides of the trough. The width of the current varies between 30 km and 45 km wide, probably because of variations in horizontal station spacing and resolution. The vertical extent is stable across the sections, with northward flow below about 2,500 m depth.

Velocity in bottom flow of the Havre Trough geostrophic flow is 1–2 cm/s. Net transport estimates from each of the four occupations of P06 indicate negligible net throughflow: 0.5Sv ±1Sv (1992), 0.3 Sv ± 0.5 Sv (2003), −0.2 Sv ± 0.5 Sv (2009), and 0.03 Sv ± 0.05 Sv for an average of 0.1 Sv. Argo float-based net transport along 32.5° across the

Havre Trough, from Colville Ridge to Kermadec Ridge, though providing limited float observations, also indicates negligible (1 Sv ± 1 Sv) net southward flow.

c. Simplified boundary current system model

Pedlosky (1994) proposed an extension to the traditional Stommel-Arons abyssal circulation model to account for leaky or gap-filled ridges along a boundary, making use of Godfrey's Island Rule (Godfrey, 1989). The model used in Pedlosky's work is a single-layer, homogeneous fluid with a forcing given by an upwelling term $w_*(x, y)$ at the layer's surface. Governing dynamics are given by the linear barotropic vorticity equation:

$$\beta v = \frac{f w_*}{H} - r\left(\frac{\partial v}{\partial x} - \frac{\partial u}{\partial y}\right), \tag{3}$$

where the advection of planetary vorticity is driven by the planetary vortex stretching given by the vertical velocity described by w_*. The frictional dissipation of vorticity, the second term on the r of the above equation, is assumed to be small and negligible everywhere outside of the boundary layer such that

$$\frac{r}{\beta L} << 1, \tag{4}$$

where L is a characteristic length scale of the size of the basin and the distribution of the upwelling, r is a frictional parameter, and β is the planetary β. The β-plane approximation is assumed to hold as well as the assumption that the velocity can be reasonably obtained from a geostrophic streamfunction, ψ, such that $u = -\frac{\partial \psi}{\partial y}$ and $v = \frac{\partial \psi}{\partial x}$.

The vorticity equation can then be written in terms of ψ

$$\beta \frac{\partial \psi}{\partial x} = \frac{f w_*}{H} - r\nabla^2 \psi, \tag{5}$$

where $\psi = \frac{p}{\rho f_0}$. Following, for the moment, the configuration of Pedlosky's example, two gaps are located at the top and bottom of the ridge while two other ridge breaks are located within the middle of the ridge system. East of the segmented ridge the interior solution takes the form of

$$\phi_I = \int_x^{x_E} -\frac{f w_*}{\beta H}(x', y)dx'. \tag{6}$$

The interior streamfunction is the westward integration of the ratio between vortex stretching due to upwelling and planetary β. Whereas on the individual ridge segments the streamfunction takes on a slightly more complicated form:

$$\phi_j = \phi_I(x, y) - (\phi_I(x_T, y) - \gamma_j)e^{-(x-x_T)/\delta}, \tag{7}$$

where $\delta = r/\beta$ is the Stommel boundary layer, ϕ_I is the interior solution of (6), and $\phi_I(x_T, y)$ is the interior solution at the ridge. The resultant streamline from this provides

a transport that may be compared with observations or other derived transport estimates. The constant γ_j is determined by an integral condition requiring that the net along-ridge frictional force vanish. It consists of the integration of the component of the momentum equation tangent to the ridge, around each ridge segment. γ_j takes the form

$$\gamma_j = \frac{1}{(y_{jN} - y_{jS})} \int_{y_{jS}}^{y_{jN}} \phi_I(x_T, y) dy. \tag{8}$$

The value of γ_j changes on each ridge segment since it is the average value of the interior ϕ_I along each segment. When $\phi_I = \gamma_j$ a stagnation point occurs on the ridge. When $\phi_I > \gamma_j$ the flow is directed to the north of the stagnation point, and when $\phi_I < \gamma_j$ the flow is turned to the south of the stagnation point. Physically, Equation 7 describes the influence of the ridge segments on the interior flow field and the anticipated decay of influence corresponding with increasing distance from the ridge.

The ridges defined in the model framework are very simple vertical walls along which the fluid rides. It is assumed that within the basin there is no topography and no sloping island skirt. This leads to a simplified model of flow control and transport. For a complete discussion of this extension see Pedlosky (1994, 1996) and Simons (2018).

To configure the model, the Lau Basin topography is idealized to two vertical, parallel ridges with openings corresponding to the passages noted in the observed data set (Fig. 2). The passages are simplified to a rectangular opening with an average depth based on the sill depth of the Tonga and Kermadec Ridges. Unlike in the Pedlosky model, no upwelling term is prescribed; instead, a non-zero eastern boundary streamline is set to represent the inflow through the Tonga Passage and the Kermadec Passage using velocities from the Argo float data set. The outflow is not prescribed at each opening on the western boundary, allowing the stream field to adjust based on the dynamics described in the model. Total inflow, however, must be balanced by the total outflow. The model results show the two westward jets observed in the Argo data. Of interest, the model also shows the southern bifurcation point of the boundary current, where a portion of the flow is directed north and the remainder southward along the ridge (Fig. 3).

In this particular model configuration, $\gamma_j \neq \gamma_{j+1}$, the ridge system is not long enough and no two stagnation points are connected by the same streamline. The recirculation regions are not completely isolated, so the pools of each recirculation communicate with the western basin through zonal jets that flow westward through the gaps in the ridge system.

d. Lau Basin boundary current transport

WBC transport in the Lau Basin was estimated from the float data, the geostrophic velocities derived from the hydrographic data, and the analytical model output. For the float data, a similar process was used as outlined in Argo and LAUBFLEX float processing. The boundary current flow was integrated laterally until the first zero velocity line, designating the lateral end of the boundary current. The same choice was used to determine the boundary

Table 1. Western boundary transport estimates within the Lau Basin derived from float data, hydrographic data, and an analytical model output.

Location	Float	Model	Hydrography
P31/North Fiji Passage	3.9	4	3.7
16.5° S	3.8	4	———
P21	4.1	3	3.8
18.5° S	2.8	3	———
19.5° S	2.0	3	———
20.5° S	4.3	3	———
21.5° S	3.8	3	———

All values reported in Sv (1 Sv = 10^6 m/s).

flow transport from the hydrographic data. The analytical model output provides a transport value on each streamline.

Forcing the inflow region of the analytical model with values similar to those observed in the inflow region of the Argo data results in boundary current transports on par with transport estimates taken from the observational data. There is good agreement between the transport estimates, with the Fiji Passage outflow transport balancing the boundary current within the Lau Basin. A total of 3–4 Sv $\pm$ 1 Sv is transported within the DWBC in the Lau Basin and exits into the North Fiji Basin.

4. Conclusions

The overall structure of the deep circulation in the Lau Basin is revealed by float measurements near 1,700 db and near 1,000 db. Geostrophic velocity estimates from the WOCE, CLIVAR, and GO-SHIP hydrographic lines together provide independent support for the presence of the WBC system along the Lau and Colville Ridges. Net transport and boundary current transport estimated from the hydrographic sections also agree well with the net transports and boundary current transports derived from the float data within the Lau Basin and the Havre Trough.

Hydrography and Argo displacement data reveal both the boundary current system in the northern part of the Lau Basin and the extension of the boundary current into the southern portion of the Lau Basin. These boundary currents are fed by two westward flowing jets located at 18° S and 27° S respectively. Zonal jets linked to gaps in ridges appear to be a common feature of deep circulation (Herbei et al. 2008); whether the zonal jets observed here have broader links to equatorial or eddy-driven dynamics (Treguier et al. 2003) is not clear.

Several areas of recirculation are present in the Lau Basin and Havre Trough. Deep water both enters and leaves the Lau Basin through the North Fiji Passage and exits the Havre Trough at depths above the ridge crest primarily through the Colville Passage. The former supplies deep water modified by recirculation in the Lau Basin to the North Fiji Basin while

the latter provides a major source at mid-depth to the South Fiji Basin. Moreover, the source of bottom water to the Havre Trough is found to be the South Fiji Basin, confirming an old suspicion of Wyrtki (1961).

Of the three regions of recirculation, two are in the Lau Basin, and one is located in the Havre Trough. In the Lau Basin both the northern and central areas of recirculation are formed by a deep flow counter to the general WBC flow direction; this flow branches at the westward jet near 17–18° S with one branch crossing underneath to continue south and close the central recirculation loop at about 22° S. Strong recirculation appears in the Havre Trough centered near 30° S. Deep circulation linked to topography is expected based on large-scale potential vorticity dynamics (O'Dwyer et al. 2000), and these flows appear to be responding to both topography and the Coriolis parameter such that they roughly follow $\frac{f}{h}$ contours. This linkage is illustrated by combining the velocity estimates from both the Argo and LAUBFLEX float observations with geostrophic contours (Fig. 10).

The observation of a flow bifurcation on the Colville Ridge, where the southern, westward-flowing jet comes into contact with the ridge provides an opportunity to test simplified dynamics of basin-scale control on boundary current systems (Pedlosky 1996; Warren and Speer 1991). An extension to the Stommel-Arons abyssal circulation model, with only inflow forcing and no interior upwelling, gives a reasonably successful, albeit simplified view of the dynamics controlling the boundary currents. Prescribing the inflow from the Argo float velocities results in boundary current transports in agreement with the estimates of boundary current transport from the Argo and LAUBFLEX floats. The analytical model also predicts the flow bifurcation and location of the bifurcation observed in the Argo float displacements.

A zonal jet bifurcation predicted by the model leads to a northward flowing boundary current that joins flow in the northern portion of the Lau Basin along the Lau Ridge and a short, southward flowing current along the Colville Ridge in the Havre Trough that exits into the South Fiji Basin. The boundary current that exits into the North Fiji Basin is observed to remain a rather tightly confined jet even after leaving the boundary.

More complex models involving interior upwelling are possible and were explored to a limited extent, but the essential information concerning major resolved currents and transport are completely contained in the model presented. The dynamics of the model involve integral theorems on the momentum and vorticity balance as developed in Pedlosky (1996) and in Equations 3–8. We believe that the simplest explanation for the boundary current structure as reflected in the present model is the most compelling one.

The regions of recirculation and other interior flow observed in the Lau Basin and Havre Trough are not, however, represented in the simplified analytical model. Interior flow requires, in the present dynamical context, a specified interior upwelling to drive it. Although the standard Stommel-Arons notion of a uniform interior upwelling provides a starting point, the presence of strong geothermal fluxes and thermal forcing in the form of hydrothermal vents generates vertical structure (Hautala and Riser 1993; Speer and Helfrich 1995; Stommel 1982) not accounted for in the simplified model.

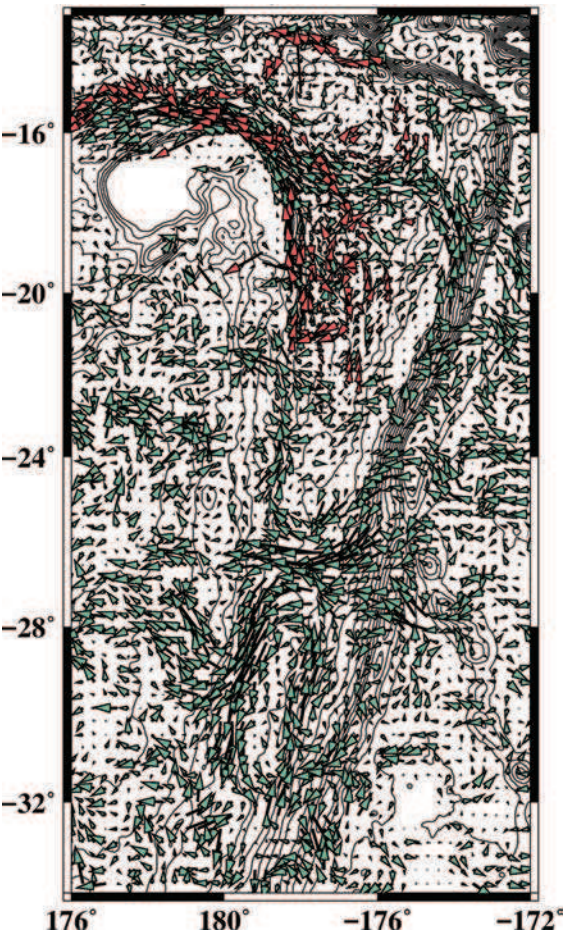

Figure 10. Lau Basin Float Experiment (LAUBFLEX) and Argo velocities on $\frac{f}{h}$ contours indicate cyclonic and anticyclonic circulation in the Lau Basin and anticyclonic circulation in the Havre Trough.

A remarkably consistent picture of the major circulation elements in the region emerges from the combined float tracks, due to a combination of boundary current dynamics and the constraints of topography. The coherence between the float displacements and the underlying topography, the depth of which varies dramatically throughout the region, is expected to be highly variable. Nevertheless, a consistent structure emerges from the data showing a vigorous deep circulation in the Lau Basin and Havre Trough, and strong exchanges of 2–4 Sv with the surrounding basins.

Acknowledgments. We gratefully acknowledge support from NSF OCE 0241785 , NSF OCE-0927583, NSF OCE 1231803, and the RIDGE 2000 program. GO-SHIP supported the 2017 P06 occupation. ES received support from The Center for Nonlinear Studies at Los Alamos National Laboratory and the Gulf Research program Deep-C.

REFERENCES

Davis, R. E. 2005. Intermediate-depth circulation of the Indian and South Pacific Oceans measured by autonomous floats. J. Phys. Oceanogr., *35*(5), 683–707. doi: 10.1175/JPO2702.1

Desbruyéres, D., J. Hashimoto, and M.-C. Fabri. 2006. Composition and biogeography of hydrothermal vent communities *in* Western Pacific Back-Arc Basins in Back-Arc Spreading Systems: Geological, Biological, Chemical, and Physical Interactions. D. M. Christie, C. R. Fisher, S.-M. Lee, and S. Givens, ed. AGU Geophysical Monography 91. Washington, DC: American Geophysical Union, 215–234.

Fornari, D., S. Beaulieu, J. Holden, L. Mullineaux, and M. Tolstoy. 2012. Introduction, *in* From RIDGE to Ridge 2000, special issue, Oceanog., *25*(1), 12–17. doi: 10.5670/oceanog.2012.01

Godfrey, J. 1989. A Sverdrup model of the depth-integrated flow for the world ocean allowing for island circulations. Geophys. Astro. Fluid., *45*, 89–112. doi: 10.1080/03091928908208894

Gray, A. R., and S. C. Riser. 2014. A global analysis of Sverdrup balance using absolute geostrophic velocities from argo. J. Phys. Oceanogr., *44*, 1213–1229. doi: 10.1175/JPO-D-12-0206.1

Hautala, S. L., and S. C. Riser. 1993. A nonconservative β-spiral determination of the deep circulation in the eastern South Pacific. J. Phys. Oceanogr., *23*, 1975–2000. doi: 10.1175/1520-0485(1993)023<1975:ANSDOT>2.0.CO;2

Herbei, R., I. McKeague, and K. Speer. 2008. Gyres and jets: Inversion of tracer data for ocean circulation. J. Phys. Oceanogr., *38*, 1180–1202. doi: 10.1175/2007JPO3835.1

Ichikawa, Y., Y. Takatsuki, K. Mizuno, N. Shikama, and K. Takeuchi. 2001. Estimation of drifting velocity and error at parking depth for the Argo float. JAMSTEC-R, *44*, 81–89.

Katsumata, K., and H. Yoshinari. 2010. Uncertainties in global mapping of Argo drift data at the parking level. J. Oceanogr., *66*, 553–569. doi: 10.1007/s10872-010-0046-4

LaCasce, J. H. 2000. Floats and f/H. J. Mar. Res., *58*, 61–95.

Lebdev, K. V., H. Yoshinari, N. A. Maximenko, and P. W. Hacker. 2007. YoMaHa'07: Velocity data assesed from trajectories of Argo floats at parking level and at the sea surface. IPRC Technical Note, *4*(2).

O'Dwyer, J., R. G. Williams, J. H. LaCasce, and K. G. Speer. 2000. Does the potential vorticity distribution constrain the spreading of floats in the North Atlantic? J. Phys. Oceanogr., *30*, 721–732.

Ollitrault, M., and J.-P. Rannou. 2013. ANDRO: An Argo-based deep displacement dataset. J. Atmos. Ocean. Technol., *30*, 759–788. doi: 10.1175/JTECH-D-12-00073.1

Park, J., K. Kim, B. King, and S. Riser. 2005. An advanced method to estimate deep currents from profiling floats. J. Atmos. Ocean. Technol., *22*, 1294–1304.

Pedlosky, J. 1996. Ocean Circulation Theory. New York: Springer.

Pedlosky, J. 1994. Ridges and recirculations: Gaps and jets. J. Phys. Oceanogr., *24*, 2703–2707.

Reid, J. L., 1997: On the total geostrophic circulation of the Pacific Ocean: Flow patterns, tracers, and transports. Prog. Oceanogr., *39*, 263–352, doi:10.1016/S0079-6611(97)00012-8.

Roemmich, D., S. Hautala, and D. Rudnick. 1996. Northward abyssal transport through the Samoan Passage and adjacent regions. J. Geophys. Res. Oceans, *101*(C6), 14039–14055. doi: 10.1029/96JC00797

Simons, E. G. 2018. Circulation in the Lau Basin and Havre Trough. Ph.D. diss., Florida State University.

Smith, W. H. F., and D. T. Sandwell, Global seafloor topography from satellite altimetry and ship depth soundings, Science, v. 277, p. 1957–1962, 26 Sept., 1997.

Speer, K., and A. Thurnherr. 2012. The Lau Basin float experiment (LAUBFLEX). Oceanogr., *35*(1), 284–285. doi: 10.5670/oceanog.2012.27

Speer, K. G., and K. R. Helfrich. 1995. Hydrothermal plumes: A review of flow and fluxes *in* Hydrothermal Vents and Processes. L. M. Parson, C. L. Walker, and D. R. Dixon, eds. London: The Geological Society, 373–386.

Stommel, H. 1982. Is the South Pacific helium-3 plume dynamically active? Earth Planet. Sci. Lett., *61*, 63–67. doi: 10.1016/0012-821X(82)90038-3

Sutton, P., S. Chiswell, R. Gorman, S. Kennan, and G. Rickard. 2012. Physical marine environment of the Kermadec Islands regions *in* Science for Conservation 318. Wellington: New Zealand Department of Conservation, 1–16.

Tivey, M., E. Becker, R. Beinart, C. Fisher, P. Girguis, C. Langmuir, P. Michael, and A.-L. Reysenbach. 2012. Links from mantle to microbe at the Lau Integrated Study Site: Insights from a back-arc spreading center. Oceanogr., *25*(1), 62–77. doi: 10.5670/oceanog.2012.04

Treguier, A.-M., N. G. Hogg, M. Maltrud, K. Speer, K., and V. Thierry. 2003. The origin of deep zonal flows in the Brazil Basin. J. Phys. Oceanogr., *33*, 580–599.

Van Dover, C. L., C. R. German, K. G. Speer, L. M. Parson, and R. C. Vrijenhoek. 2002. Evolution and biogeography of deep-sea vent and seep invertebrates. Science, *295*(5558), 1253–1257. doi: 10.1126/science.1067361

Warren, B. A., and K. G. Speer. 1991. Deep circulation in the eastern South Atlantic Ocean. Deep Sea Res., *38*(suppl.), 281–322.

Warren, B. A., T. Whitworth III, M. I. Moore, and W. D. Nowlin, Jr. 1994. Slight northwestward inflow to the deep South Fiji Basin. Deep Sea Res. I, *41*(5/6), 953–956.

Whitworth III, T., B. A. Warren, W. D. Nowlin Jr., S. B. Rutz, R. D. Pillsbury, M. I. Moore, W. Nowlin, Jr., S. B. Rutz, R. D. Pillsbury, and M. I. Moore. 1999. On the deep western-boundary current in the Southwest Pacific Basin. Prog. Oceanogr., *43*(1), 1–54.

Wijffels, S. E., J. M. Toole, and R. Davis. 2001. Revisiting the South Pacific subtropical circulation: A synthesis of World Ocean Circulation Experiment observations along 32° S. J. Geophys. Res., *106*(C9), 19481. doi: 10.1029/1999JC000118

World Ocean Database 2013. 2013. NOAA Atlas NESDIS 72. Accessed 20 February 2020. https://repository.library.noaa.gov/view/noaa/1291

Wyrtki, K. 1961. The flow of water into the deep sea basins of the western South Pacific Ocean. Aust. J. Mar. Freshwater Res., *12*(1), 1–16.

Received: *4 January 2019*; revised: *12 February 2020*.